https://doi.org/10.5194/esurf-2022-52
Preprint. Discussion started: 20 September 2022

Earth Surface Dynamics Discussions

Method to evaluate large wood behavior in terms of convection equation associated with sediment erosion and deposition

Daisuke HARADA[1], Shinji EGASHIRA[1]

[1]International Centre for Water Hazard and Risk Management (ICHARM), Public Works Research Institute (PWRI), 1-6, Minamihara, Tsukuba, Ibaraki, 305-8516, Japan

Correspondence to: Daisuke HARADA (d-harada55@pwri.go.jp)

Abstract. This paper proposes a method for describing large wood behavior in terms of the convection equation and the storage equation, which is associated with active sediment erosion and deposition. Recent flood hazards are characterized by numerous amounts of sediment and large wood supplied from upstream mountainous areas, which often exacerbate flood disasters in downstream areas. Previous studies proposed methods to simulate large wood behavior by tracking the motion of individual wood pieces in the flood flow using the Lagrangian method. This study aims to propose a method to simulate the behavior of large amounts of large wood in the flow field with active sediment transportation by employing the convection equation and the storage equation with sediment erosion and deposition to simulate the behavior of numerous numbers of large wood pieces. The proposed method is applied to simulate the flood flow with numerous amounts of sediment and large wood in the Akatani river flood disaster, 2017, where the production and transport processes of sediment and large wood from the basin during heavy rainfall events are employed as upstream boundary conditions for the flood flow analysis. The 2-D flood flow computations indicate that the flood flow can be significantly affected by the large wood deposition at the bridge in terms of water level, velocity distribution, and sediment deposition. The comparison between the field and simulation results addressing large wood deposition in the field demonstrates that the simulation method proposed in this study can reproduce large wood behavior successfully. Overall, since the proposed method makes it possible to simulate the behavior of a numerous number of large wood, it can be applied to the management of hazards, such as the Akatani River.

1 Introduction

On July 5th, 2017, Northern Kyusyu in Japan experienced extremely heavy rainfall, which caused landslides and debris flows at numerous locations in its mountainous regions. The landslides and debris flows generated numerous amounts of sediment and large wood. Once these sediment and large wood were deposited in the river channel, they were transported downstream by the flood flow. In downstream areas, large wood accumulation took place at many locations, such as bridges and sediment deposition areas and influences the flood flow (Chen et al., 2018; Harada and Egashira, 2018). Recently, these types of flood hazards have been reported in numerous places in steep, forested areas (Lucía et al., 2015; Lucía et al., 2018; Steeb et al., 2017; Comiti et al., 2016; Harada et al., 2019). As reported in these studies, large wood often becomes a major contributing factor

https://doi.org/10.5194/esurf-2022-52
Preprint. Discussion started: 20 September 2022

that exacerbates flood disasters. Hence, it is of high importance to develop an evaluation method for the behavior of large wood in a flood flow.

According to the reflections of the research history on large wood in rivers (Swanson et al., 2021; Ruiz-Villanueva et al., 2019), previous studies have proposed simulation models for large wood behavior. Nakagawa et al. (1994) proposed a numerical simulation model to compute the behavior of individual wood pieces in a two-dimensional flow field by calculating the transportation of driftwood using a combination of translocation and rotation. This method was applied and verified in several laboratory experiments (Shrestha et al., 2009; Shrestha et al., 2012). Gotoh (2001) proposed a method to track the motion of driftwood based on the LaGrange particle method (MPS method) by treating wood pieces as a rigid body. Shimizu et al. (2006) developed a model composed of two types of analyses: the Eulerian analysis of fluid motion, given by depth-averaged flow analysis, and the Lagrange analysis of driftwood motion, using the extended distinct element method. Ruiz-Villanueva et al. (2014) proposed a method to compute the transport of individual large wood pieces in a two-dimensional flow field, including physical modeling of the wood recruitment process to the flood flow. Kimura et al. (2021) developed models to compute large wood motion in a three-dimensional flow field.

In addition to those proposed methods for tracking the motion of wood pieces in the flow field, some researches have proposed methods to analyze large wood production processes at a basin scale. Mazzorana et al. (2009) proposed methods to estimate large wood production processes in mountainous streams by a GIS-based index. Mazzorana et al. (2011) proposed a model for wood entrainment and deposition processes based on empirical methods and the transportation of wooden materials in the flow field. Komori et al. (2021) proposed a model to evaluate large wood export at a watershed scale.

Although those research ranges from the basin scale large wood production to the models tracking the motion of individual wood pieces in the flood flow based on the Lagrangian method, it is difficult to apply these methods to flood disasters, such as the 2017 flood disaster in Northern Kyusyu, because in these events, numerous numbers of large wood pieces were produced in the mountains by landslide and debris flows, and that were transported through river channels in the flood flow. Therefore, it is also necessary to develop a method to simulate the behavior of a huge amount of large wood in the flow field with active sediment transportation and bed deformation. The present paper proposes a numerical method to describe the behavior of large wood based on the convection equation and the storage equation with sediment erosion and deposition to simulate the behavior of numerous numbers of large wood pieces. We also propose methods to evaluate a basin scale sediment and large wood production and its transportation, and then using this as a boundary condition to calculate flood flows at downstream, we investigate how large wood behavior, e.g., wood capture at bridges, affects flood flows and sediment deposition in the surrounding area. The proposed model has been applied to the 2017 flood disaster in Northern Kyusyu to reveal the effect of large wood behavior on the flood flow.

https://doi.org/10.5194/esurf-2022-52
Preprint. Discussion started: 20 September 2022

Earth Surface Dynamics Discussions
Open Access
EGU

2 Methods

In our proposed methods, the flow field is simulated using 2-D depth-integrated governing equations, which include mass and momentum conservation equations. The equations are expressed in the Cartesian coordinate system as follows:

$$\frac{\partial h}{\partial t}+\frac{\partial uh}{\partial x}+\frac{\partial vh}{\partial y}=0 \tag{1}$$

$$\frac{\partial hu}{\partial t}+\frac{\partial huu}{\partial x}+\frac{\partial huv}{\partial y}=-gh\frac{\partial(h+z_b)}{\partial x}-\frac{\tau_x}{\rho}+\frac{1}{\rho}\left(\frac{\partial h\sigma_{xx}}{\partial x}+\frac{\partial h\tau_{yx}}{\partial y}\right) \tag{2}$$

$$\frac{\partial hv}{\partial t}+\frac{\partial huv}{\partial x}+\frac{\partial hvv}{\partial y}=-gh\frac{\partial(h+z_b)}{\partial y}-\frac{\tau_y}{\rho}+\frac{1}{\rho}\left(\frac{\partial h\tau_{xy}}{\partial x}+\frac{\partial h\sigma_{yy}}{\partial y}\right) \tag{3}$$

where x and y are the coordinates in the major flow direction and normal to the flow direction, respectively; t is the time; h is the flow depth; u and v are the x and y components of the depth-averaged velocity; g is the acceleration due to gravity; ρ is the mass density of water; σ_{xx}, σ_{yy}, τ_{xy}, and τ_{yx}, are the depth-averaged Reynolds stresses; z_b is the bed elevation; τ_x and τ_y are the x and y components of the bed shear stress, respectively.

Equations (1) to (3) are transformed into a general coordinate system (Shimizu and Itakura, 1991). The equations are numerically calculated by the cubic interpolated pseudo-particle (CIP) method (e.g., Yabe et al., 1991, Jang and Shimizu, 2005).

The processes of bed deformation and suspended sediment transport in the flow field are computed using the following equations:

$$\frac{\partial z_b}{\partial t}+\frac{1}{1-\lambda}\sum_i\left(\frac{\partial q_{bix}}{\partial x}+\frac{\partial q_{biy}}{\partial y}+E_i-D_i\right)=0 \tag{4}$$

$$\frac{\partial c_i h}{\partial t}+\frac{\partial uc_i h}{\partial x}+\frac{\partial vc_i h}{\partial y}=E_i-D_i \tag{5}$$

where λ is the porosity of the bed sediment; q_{bix} and q_{biy} are the x and y components of the bedload transport rate for grain size d_i, respectively; E_i and D_i are the erosion and deposition rates of the suspended sediment for grain size d_i, respectively, c_i is the depth-averaged suspended sediment concentration for grain size d_i.

The bedload transport rate is estimated using a formula developed by Egashira et al. (1997), in which the constitutive relations of a water-sediment mixture flow are applied to the bedload layer.

$$q_{b*i}=\frac{4}{15}\frac{{K_1}^2K_2}{\sqrt{f_d+f_f}}{\tau_{*i}}^{5/2}p_i \tag{6}$$

where q_{b*i} is the non-dimensional bedload transport rate for grain size d_i; τ_{*i} is the non-dimensional tractive force for grain size d_i; p_i is the content ratio for grain size d_i; the other parameters, K_1, K_2, f_d, and f_f, are specified based on Egashira et al. (1997).

https://doi.org/10.5194/esurf-2022-52
Preprint. Discussion started: 20 September 2022


Earth Surface Dynamics Discussions Open Access EGU

$$K_1 = \frac{1}{\cos\theta}\,\frac{1}{\tan\phi_s - \tan\theta} \tag{7}$$

$$K_2 = \frac{1}{\overline{c_s}}\left[1 - \frac{h_s}{h}\right]^{1/2} \tag{8}$$

$$f_d = k_d(1-e^2)\frac{\sigma}{\rho}\overline{c_s}^{1/3} \tag{9}$$

$$f_f = k_f(1-\overline{c_s})^{5/3}\overline{c_s}^{-2/3} \tag{10}$$

where θ is the local slope; ϕ_s is the angle of repose; $\overline{c_s}$ is the sediment concentration on the bedload layer; h is the water depth; σ is the density of soil particle; ρ is the density of water; e is the coefficient of restitution; k_d=0.0828; k_f=0.16∼0.25. Indeed, most of the values in equations (7) to (10) are regarded as constant in the flow field described by equations (1) to (3), thus assuming, $\phi_s = 34°$, $\overline{c_s} = 0.25$, $h_s \approx h$, the value of the term $4/15\ {K_1}^2 K_2/\sqrt{f_d + f_f}$ in equation (6) is approximately 3.8.

In equation (8), h_s is the thickness of the bedload layer, which is described as follows:

$$\frac{h_s}{h} = \frac{1}{(\frac{\sigma}{\rho}-1)\overline{c_s}}\,\frac{\tan\theta}{\tan\phi_s - \tan\theta} \tag{11}$$

The grain size distribution of bed materials is evaluated based on the concept of the bedload layer, the transition layer, and the deposition layer, which was developed by Luu et al. (2006), assuming that the mass of each material is preserved.

Erosion rate E_i of suspended sediment in equations (4) and (5) are evaluated using the following equations proposed by Harada et al. (2022);

$$E_i = p_i W_e \overline{c_s} \tag{12}$$

$$\frac{W_e}{U} = \frac{K}{R_{i*}} \tag{13a}$$

$$R_{i*} = (\sigma/\rho - 1)\overline{c_s} g h/U^2 \tag{13b}$$

where W_e is the entrainment velocity, U is the flow velocity, i.e., $x = \sqrt{u^2+v^2}$, R_{i*} is the overall Richardson number, c is the depth-averaged suspended sediment concentration, and $K = 1.5 \times 10^{-3}$ (Egashira and Ashida, 1980).

To analyze numerous amounts of large wood in the flood flow, it is assumed that wood pieces behave as neutral buoyant particles, for this assumption enables the introduction of the convection equation. Further, assuming that the erosion and deposition of large wood take place in proportion to sediment erosion and deposition and also assuming that large wood accumulation occurs at artificial structures such as bridges, the convection equation is coupled with the storage equation of large wood in the channel bed. Based on these assumptions, the behavior of large wood in the flood flow is expressed using the following equations:

$\partial z_b/\partial t > 0$:

https://doi.org/10.5194/esurf-2022-52
Preprint. Discussion started: 20 September 2022


Earth Surface Dynamics Discussions
Open Access
EGU

$$\frac{\partial c_{drf} h}{\partial t} + \frac{\partial c_{drf} uh}{\partial x} + \frac{\partial c_{drf} vh}{\partial y} = -c_* \frac{\partial z_b}{\partial t} c_{drf} r(t,x,y) - v_n c_{drf} p_b \delta(x - x_i, y - y_i) \quad (14)$$

$$\frac{\partial S}{\partial t} = \frac{\partial z_b}{\partial t} c_{drf} r(t,x,y) + v_n c_{drf} p_b \delta(x - x_i, y - y_i) \quad (15)$$

$\partial z_b/\partial t<0$:

$$\frac{\partial c_{drf} h}{\partial t} + \frac{\partial c_{drf} uh}{\partial x} + \frac{\partial c_{drf} vh}{\partial y} = -c_* \frac{\partial z_b}{\partial t} \frac{S}{D} r(t,x,y) - v_n c_{drf} p_b \delta(x - x_i, y - y_i) \quad (16)$$

$$\frac{\partial S}{\partial t} = \frac{\partial z_b}{\partial t} \frac{S}{D} r(t,x,y) + v_n c_{drf} p_b \delta(x - x_i, y - y_i) \quad (17)$$

where c_{drf} is the depth-averaged large wood concentration; c_* is the sediment concentration of the stationary bed; v_n is the inward velocity normal to the structure area such as the bridge; D is the depth of the standing tree's root; S is the storage of large wood on the ground or the riverbed per unit area; when the volume of a piece of wood is V (m^3), S and the number of wood (N) in a certain area (A m^2) is converted by $S = VN/A$ (m).

Equations (14) and (16) are the convection equations for the large wood transport with the water flow, and equations (15) and (17) are the storage equations of large wood stored on the bed. The first term of the right-hand side in equations (14) to (17) represents large wood exchange between the water and the bed. Since we assume that the erosion and deposition of large wood take place in proportion to sediment erosion and deposition, the term in equations (14) and (15) represents the wood deposition from the water to the bed, and the term in equations (16) and (17) represents the large wood recruitment from the bed to the water. Figure 1 (a) shows the concept of such processes.

In the case of sediment deposition, $c_* \partial z_b/\partial t$ corresponds to the height of sediment deposition per unit time. We assume the large wood contained within the height is deposited to the riverbed, thus the amount of $c_* \partial z_b/\partial t \; c_{drf}$ is stored in the riverbed. In the case of sediment erosion, as shown in Figure 1 (b), when the bed erosion reaches the root depth D, all of the wood storage S is recruited to the water. Therefore, $S \; c_* \partial z_b/\partial t \; /D$ corresponds to the large wood recruitment from the bed to the water per unit time.

Meanwhile, the large wood recruitment does not occur at depths shallower than a certain water depth and the large wood deposition will not occur at depths deeper than a certain water depth. $r(t,x,y)$ in equations (14) to (17) are introduced to describe such cases, and the function $r(t,x,y)$ in the present research is set as shown in Figure 2.

In Eqs. (14) and (16), the last term defines large wood capture at the bridge. Dirac's δ-function is employed to evaluate the capturing of large wood at structures such as bridges by defining the locations of these types of structures as $((x, y) = (x_i, y_i))$ and setting Dirac's δ-function for the structures as δ = 1 and for other places as δ = 0. p_b denotes the probability that large wood is captured at structures, ranging from 0 to 1.

When a large wood deposition occurs, the sediment transport rate may be reduced due to the hiding effect of large wood deposition. Therefore, in the present study, the bedload transport rate in equation (6) and the erosion rate of suspended sediment in equation (12) are reduced at the rate of its hiding effect.

https://doi.org/10.5194/esurf-2022-52
Preprint. Discussion started: 20 September 2022

At a point where a structure, such as a bridge, exists, e.g., $((x, y) = (x_i, y_i))$, the cross-sectional area occupied by the water decreases. In these areas, the velocities across the cell, i.e., $u\Delta x$ and vΔy, are reduced by $u\alpha\Delta x$ and vαΔy, where α is described as follows:

$$\alpha = \frac{S}{h}/(1 - c_{*drf}) \tag{18}$$

where c_{*drf} is the wood concentration of a stationary layer composed of the deposited large wood only.

3 Numerical simulations

3.1 Target areas and hazard characteristics

Numerical simulations of the flood flow with sediment and large wood are conducted for the Akatani River basin, which is located on the right-bank side of the Chikugo River, where a large amount of sediment and large wood was produced in the 2017 flood disaster in Northern Kyusyu, Japan. The drainage area and the stream length of the Akatani River are approximately 20 km2 and 8 km, respectively. According to Nagumo & Egashira (2019), 639 houses or buildings in the basin were damaged during the event. Figure 3 shows the Akatani River basin with debris flows and flood marks identified from aerial photos. This shows that numerous landslides and debris flows occurred in the mountainous areas, which increased damage to the downstream areas. Figure 4 compares aerial photos taken before and after the disaster. Although it is difficult to identify the river channel in the photo before the event because of its very narrow width, sediment widely spread over the valley bottom in the photo after the event, indicating highly active sediment transport and deposition during the event.

Figure 5 shows the sediment size distribution observed immediately after the flood event. Longitudinal sediment sorting is clearly observed, exhibiting a tendency of the sediment size becoming finer towards downstream. Moreover, although the average bed slope of the Akatani River is approximately 1/70, the grain size of the deposited sediment is quite fine, which indicates that a large amount of fine sediment was supplied from the upstream area during the event.

During the flood event, numerous amounts of large wood were supplied to the channels. Figure 6 shows the distribution of deposited wood length, which is identified from aerial photos taken just after the event. Three areas along the Akatani River channel and one valley in the basin are selected to investigate the length of each wood piece, for the resolution of the aerial photos taken for these areas is sufficient for this purpose. According to Figure 6, the distribution of wood length decreases from the inside of the valley to its downstream area. Some of the large wood deposited in the downstream end of the valley may have been transported to downstream reaches and deposited along the Akatani River channel.

3.2 Upstream boundary conditions

To conduct a 2-D depth-integrated analysis under the conditions such as the Akatani river disaster, it is necessary to evaluate the amount of sediment and large wood inflow from the basin at the upstream boundary of the 2-D analysis area. In this study, we obtained the upstream boundary condition by an integrated method to simulate rainfall-runoff, landslide and debris flow,

https://doi.org/10.5194/esurf-2022-52
Preprint. Discussion started: 20 September 2022

and sediment and large wood transport in the river channel to obtain a time series of sediment and large wood discharged from the basin (Harada et al., 2022).

The occurrence of landslide, debris flow, and large wood transport induced by the landslide on the hill slope are evaluated based on the method of Yamazaki et al. (2019). Slope stability analysis to evaluate the landslide occurrence is performed in the slope cell of the Rainfall-runoff-inundation (RRI) model developed by Samaya et al., (2012). Parameters employed for the rainfall-runoff and landslide calculations are shown in Table 1. As for the water discharge, since the flow discharge was not observed during the event, the same parameters are applied to the Akatani river basin by performing the calibration on the Kagetsu river, which locates next to the river to the east, and confirmed that the result for peak discharge in the Akatani river is not significantly different from those in other reports, (e.g., Shakti et al. (2018)). The initial conditions of sediment size distribution in each unit channel are shown by the green dotted line in Figure 5. As for the large wood runoff computation from the basin, referring to the authors survey and Kubota (2019), assuming the average diameter of a standing tree 15cm, the length is 11.2m, and the standing tree density as one tree in $2m^2$, the density of standing trees is set as 0.06 (m^3/m^2). It is assumed that these trees are transported and supplied to the nearest unit channel when the landslide and debris flow occurs.

The sediment transport that accompanies the landslide is analyzed using the equation of a mass system, from the point of origin to the location where the deposition occurs, and when the sediment reaches the river channel, it is treated as sediment supply into the channel. In the river channel, sediment and large wood transport is evaluated with the methods proposed by Egashira and Matsuki (2000), in which a section that includes the upstream confluence and excludes the downstream confluence point is designated as the unit channel, and the sediment and large wood runoff for the entire basin is predicted by allocating the unit channels in series and parallel. As for the large wood transport in the channel network, the behavior of the large wood in the unit channel follows the one-dimensional forms of equations (14)-(17).

The upstream boundary conditions obtained using this method are shown in Figure 7. The Figure shows the temporal variation of the basin scale computational results for flood water, suspended sediment, and large wood discharge at the 3.5 km point; the location corresponds to the upstream boundary of the 2-D flood flow computation. According to the figure, suspended sediment and large wood discharge are concentrated before the flow discharge peak comes.

3.3 Computational conditions for the 2-D flood flow with sediment and large wood behavior

The computation area is approximately 3.5 km long, as shown in Figure 3. The average bed slope of the computational domain is approximately 1/120. For the computation, iRIC-Nays2DH (Shimizu et al., 2019), which was partially modified by the authors, is employed. As the initial topography, DEM data measured by an aerial laser survey before the flooding is used. The roughness coefficient is set as 0.03 for the entire computation domain. The initial sediment size distribution, indicated by the green dotted line in Figure 5, is given for the entire computed domain. No large wood is assumed to be initially deposited (S=0 in Eqs. (14)-(17)) in the entire calculation domain.

Seven bridges inside the domain were set as obstacles, and $\delta = 1$ in equations (14)-(17) at these locations. The large wood capture rate p_b at bridges can take values between 0 and 1, but in this study, p_b is uniformly set to 1. In this computation, when

https://doi.org/10.5194/esurf-2022-52
Preprint. Discussion started: 20 September 2022

large wood accumulation takes place on bridges, the cross-section area of the flow in the grid is reduced, which in turn affects the flow conditions around the bridges. Calculations are performed for the three cases shown in Table 2 to compare the differences in results depending on the presence of sediment and large wood.

4 Computation results

Figure 8 compares Cases 1, 2, and 3, and shows a water depth contour map at the peak discharge time, that shows the are between 1.2 km and 2.5 km from the downstream end of the computational domain. For example, the area circled by the solid white line in Figure 8 shows that a wider area is inundated in Case 3 than in Case 1, which is closer to the actual inundated area.

Figure 9 compares the difference between the ground elevation measured by an aerial laser survey before and after the flooding (left figure) and the difference between the beginning and the end of the calculation for the ground elevation in Case 3 (right figure). Although the calculation results show a little excessive sediment deposition at around upstream of 1.5 km point, the two trends are generally consistent in terms that more than 2m sediment deposition takes place in the river channel and that sediment is deposited several tens of centimeters to 1m thick in the areas where inundation occurred.

Figure 10 compares the number of pieces of computed large wood deposition in a 25-m square area with the number of pieces deposited in the field at the end of the calculation. The computed results, i.e., S in equations (14)-(17), are converted to the number of pieces of large wood by assuming that the diameter and length of a piece of wood are 20 cm and 7 m, respectively, referring to Figure 6 and Kubota (2019). The number of pieces of large wood deposited within a 25-m square area is deciphered from aerial photographs taken immediately after the flood event. According to the figure, although it should be noted that some of the large wood may be undecipherable because it is buried and not surfaced despite being deposited, the trend of large wood deposition in the area is generally consistent.

5 Discussions

This section provides a more detailed discussion concerning the impact of large wood on flood flows, and the characteristics of the proposed method in this study.

Figure 11 shows the results for each case for the water level in the river channel and the riverbed height at the peak flow, and the results are compared with the water level mark. In Case 3, the accumulation of large wood near the bridge obstructs the river channel flow, thus the water level rises markedly upstream of the bridge. Comparing the water level mark and the calculated water level around 1.5 km, the water levels in Cases 1 and 2 are about 1 m lower than the water level mark, and the water level in Case 3 is about 1 m higher than the water level mark. The higher water level in Case 3 is partly due to the large wood capture rate p_b at the bridge is uniformly set to 1, but at least the water level is evaluated lower in Cases 1 and 2, where large wood is not considered. In Case 3, the bed shear stress in the river channel is reduced at upstream of the bridge, that

https://doi.org/10.5194/esurf-2022-52
Preprint. Discussion started: 20 September 2022

causing significant sediment deposition here. Figure 11 shows that in Case 3, a large amount of sediment has already deposited in the river channel before the peak flow, which significantly reduces the channel capacity before the peak flow comes. In Case 2, sediment deposition in the river channel is also significant; however, the amount of sediment deposition is not as large as in Case 3 because the deposition of large wood on the bridge and the associated flow obstructions are not calculated. Due to these effects, the flood inundation extends over the valley bottom, as is especially noticeable near the bridge in Case 3 in Figure 8.

Figure 12 shows the contours of the flow velocity in the vicinity of the bridge (1.2 to 1.5 km). Figure 12 compares Case 2, in which large wood is not computed, with Case 3, in which large wood is computed. The flow is obstructed in the bridge due to the large wood accumulation at the bridge, causing the flow to divert around it. This results in a larger area of inundation in Case 3 and a larger area subject to higher velocity fields.

With regard to the the spatial distribution of large wood deposition, comparison of figures between the left figures in Figure 9 and 10, the locations where sediment is deposited with a thickness of several tens of centimeters to one meter and the locations where large wood is deposited generally coincide. This indicates that the modeling in this study, in which erosion and deposition of large wood occur in response to erosion and deposition of sediment, has a certain appropriateness.

The present paper has proposed a new approach to simulate the behavior of large wood in the flow field based on the convection-diffusion equation. The approach is particularly useful in cases requiring a numerous number of large wood behavior simulations because it is impractical to employ the Lagrangian approach when such numerous amounts of large wood are supplied, as in the case of the Akatani River. The method is also beneficial in simulating large wood accumulation at structures such as bridges. On the other hand, since the large wood deposition on the riverbed and the amount of large wood captured by bridges depend on the functional form $r(t,x,y)$ and the capture rate p_b, the method for setting these parameters should be studied further. In other words, the exchange of large wood from the water to the riverbed or from the water to the bridge is still a difficulty to the application of this study, and this point requires further research in the future.

6 Conclusion

The present paper has proposed a method to simulate the behavior of large wood in the flow field based on the convection equation and the storage equation with active sediment transportation and channel bed deformation, which characterizes recent flood disasters in mountainous and hilly regions, such as the flood disaster in the Akatani river in 2017. The proposed method is applied to simulate the flood flow with numerous amounts of sediment and large wood in the Akatani river flood disaster.

From the results of 2-D flood flow computations with sediment and large wood, we found that the observed sediment and large wood deposition correspond well with the calculation results. The comparison of large wood deposition between the field and simulation results shows that the simulation can reproduce a tendency of large wood deposition in the field, although the wood piece distribution by aerial photos is not perfectly accurate, as some large wood pieces are buried in the riverbed or lay under other pieces.

https://doi.org/10.5194/esurf-2022-52
Preprint. Discussion started: 20 September 2022

The calculation results are significantly different when the effects of sediment and large wood are considered, indicating that it is essential to consider these factors in the analysis. In particular, when large wood is captured in a bridge, the obstruction of the flow causes the flow diversion around the bridge, which significantly affects the flow pattern and river bed deformations above around the bridge. In this model, the erosion and deposition of large wood, as well as the large wood capture rate at the bridge, are factors that significantly affect the calculation results and these will require further study.

Since the proposed method makes it possible to simulate the behavior of a large number of driftwood pieces, it can be applied to the management of hazards, such as the Akatani river. The computed results are useful for obtaining the effectiveness of countermeasures, developing hazard maps, and evacuation plans. In addition, the effect of countermeasures such as large wood capturing structures can be evaluated through simulations using the proposed method, which provides practical information to control hazards more efficiently and effectively.

Data availability

The data used in this study are freely available from the corresponding author upon request.

Author contributions

DH and SE designed the study. DH performed the numerical simulations, and wrote the paper. SE reviewed and edited the paper.

Competing interests

The authors declare that they have no conflict of interest.

Acknowledgements

The authors would like to thank Dr. Nagumo, N., Mr. Nakamura, Y. and Dr. Yamazaki, Y. for their contribution to field survey and data preparation.

Financial support

This work was supported by JSPS KAKENHI Grant Number 22K14334.

https://doi.org/10.5194/esurf-2022-52
Preprint. Discussion started: 20 September 2022

References

Chen, X., Hirakawa, R., & Ohmoto, T.: Numerical Analysis of Effect of Bridge on Inundation Flow in the Kagetsu River on July 2017. International Journal of Environmental Protection and Policy, 6(4), 78-84. doi: 10.11648/j.ijepp.20180604.12, 2018.

Comiti, F., Lucía, A., & Rickenmann, D.: Large wood recruitment and transport during large floods: a review. Geomorphology, 269, 23-39, doi:10.1016/j.geomorph.2016.06.016, 2016.

Egashira, S., and Ashira, K.: Studies on the Structures of Density Stratified Flows., Bulletin of the Disaster Prevention Research Institute, Kyoto University, 29(4), pp.165-198, 1980.

Egashira, S. and Matsuki, T.: A method of predicting sediment runoff caused by erosion of stream channel bed. Annual Journal of Hydraulics Engineering, Japan Society of Civil Engineers, 44, 735–740, 2000 (In Japanese).

Gotoh, H.: Sub-particle-scale turbulence model for the MPS method-Lagrangian flow model for hydraulic engineering. Computational Fluid Dynamics Journal, 9(4), pp.339-347, 2001.

Harada, D. & Egashira, S.: Flood flow characteristics with fine sediment supply and drift woods -analysis on the akatani river flood hazards in july, 2017-, Annual Journal of Hydraulic Engineering, JSCE, vol.74: I_937-I_942, 2018 (In Japanese).

Harada, D., Nagumo, N., Nakamura, Y., Egashira, S.: Characteristics of Flood Flow with Active Sediment Transport in the Sozu River Flood Hazards at the Severe Rainfall Event in July 2018., Journal of Disaster Research 14.6, pp.886-893, doi:10.20965/jdr.2019.p0886, 2019.

Harada, D., Egashira, S., Ahmad, T. S., & Ito, H.: Entrainment of bed sediment composed of very fine material, Eath Surface Process and Landforms, Advance online publication. doi:10.1002/esp.5442, 2022.

Harada, D., & Egashira, S.: Methods to analyse flood flow with a huge amount of sediment and driftwood, Advances in river engineering, JSCE, 28, 289-295, 2022 (In Japanese).

Jang, C. L., & Shimizu, Y.: Numerical simulations of the behaviour of alternate bars with different bank strengths. Journal of Hydraulic Research, 43(6), 596-612, doi:10.1080/00221680509500380, 2005.

Kimura, I., Kang, T., & Kato, K.: 3D–3D Computations on Submerged-Driftwood Motions in Water Flows with Large Wood Density around Driftwood Capture Facility. Water, 13(10), 1406, doi:10.3390/w13101406, 2021.

Komori, D., Sukegawa, Y., Chaithong, T., & Kazama, S.: Modelling of large wood export at a watershed scale. Earth Surface Processes and Landforms, 47(2), 688-696, doi:10.1002/esp.5282, 2022.

Kubota, T.: Elucidation of the Characteristics of Forest Slope Landslides and Woody Debris Disaster Induced by the Northern Kyushu Big Downpours in 2017. Water science, 62(6), 10-12, doi:10.20820/suirikagaku.62.6_10, 2019, (In Japanese).

Lucía, A., Comiti, F., Borga, M., Cavalli, M., & Marchi, L. Dynamics of large wood during a flash flood in two mountain catchments. Natural Hazards and Earth System Sciences, 15(8), pp.1741-1755. doi:10.5194/nhess-15-1741-2015, 2015.

Lucía, A., Schwientek, M., Eberle, J., & Zarfl, C.: Planform changes and large wood dynamics in two torrents during a severe flash flood in Braunsbach, Germany 2016. Science of the Total Environment, 640, pp.315-326, doi:10.1016/j.scitotenv.2018.05.186, 2018.

https://doi.org/10.5194/esurf-2022-52
Preprint. Discussion started: 20 September 2022

Luu, X. L., Egashira, S., & Takebayashi, H.: A new treatment of the exchange layer thickness to evaluate sediment sorting and armoring. Journal of applied mechanics, 9, 1025-1030, doi:10.2208/journalam.9.1025, 2006.

Mazzorana, B., Zischg, A., Largiader, A., & Hübl, J.: Hazard index maps for woody material recruitment and transport in alpine catchments. Natural Hazards and Earth System Sciences, 9(1), 197-209, doi:10.5194/nhess-9-197-2009, 2009.

Mazzorana, B., Hübl, J., Zischg, A. M., Largiader, A.: Modelling woody material transport and deposition in alpine rivers, Natural Hazards 56(2): 425–449, doi:10.1007/s11069-009-9492-y, 2011.

Nakagawa H., Takahashi T., and Ikeguchi M.: Numerical simulation of drift wood behavior. Disaster Prevention Research Institute Annuals, Vol. 35 B-2, pp. 249-266, 1994 (In Japanese).

Nakamura, Y., Ikeuchi, K., Abe, S., Koike, T., & Egashira, S.: Evaluation of the uncertainty of flash flood prediction using the RRI model in mountainous rivers. EPiC Series in Engineering, 3, 1486-1494, doi:10.29007/n72w, 2018.

Nagumo, N. & Egashira, S.: Flood Hazard Analysis and Locations of Damaged Houses Based on Land Classification in the Akatani River Basin Following Torrential Rainfall in Northern Kyushu, 2017, Journal of Geography（Chigaku Zasshi）,128（6）, pp.835-854, doi:10.5026/jgeography.128.835, 2019 (In Japanese).

Ruiz-Villanueva, V., Bladé, E., Sánchez-Juny, M., Marti-Cardona, B., Díez-Herrero, A., & Bodoque, J. M.: Two-dimensional numerical modeling of wood transport. Journal of Hydroinformatics, 16(5), 1077-1096, doi:10.2166/hydro.2014.026, 2014.

Ruiz-Villanueva, V., Mazzorana, B., Bladé, E., Bürkli, L., Iribarren-Anacona, P., Mao, L., Nakamura, F., Ravazzolo, D., Rickenmann, D., Sanz-Ramos, M. and Stoffel, M.: Characterization of wood-laden flows in rivers. Earth Surface Processes and Landforms, 44(9), pp.1694-1709, doi:10.1002/esp.4603, 2019.

Sayama, T., Ozawa, G., Kawakami, T., Nabesaka, S., & Fukami, K.: Rainfall–runoff–inundation analysis of the 2010 Pakistan flood in the Kabul River basin. Hydrological Sciences Journal, 57(2), 298-312, doi:10.1080/02626667.2011.644245, 2012.

Shakti P.C., Nakatani, T., & Misumi, R.: Hydrological simulation of small river basins in northern Kyushu, Japan, during the extreme rainfall event of July 5–6, 2017. Journal of Disaster Research, 13(2), 396-409, doi:10.20965/jdr.2018.p0396, 2018.

Shrestha, B. B., Nakagawa, H., Kawaike, K., Baba, Y., & Zhang, H.: Numerical simulation on debris-flow with driftwood and its capturing due to jamming of driftwood on a grid dam. Annual Journal of Hydraulic Engineering, JSCE, 53, 169-174, 2009.

Shrestha, B. B., Nakagawa, H., Kawaike, K., Baba, Y., & Zhang, H.: Driftwood deposition from debris flows at slit-check dams and fans. Natural Hazards, 61(2), 577-602, doi:10.1007/s11069-011-9939-9, 2012.

Shimizu, Y., & Itakura, T.: Calculation of flow and bed deformation with a general non-orthogonal coordinate system, Proceedings of XXIV IAHR Congress, Madrid, Spain, C-2 , pp. 41-48, 1991.

Shimizu, Y., Nelson, J., Arnez Ferrel, K., Asahi, K., Giri, S., Inoue, T., Iwasaki, T., Jang, C.L., Kang, T., Kimura, I. and Kyuka, T.: Advances in Computational Morphodynamics Using the International River Interface Cooperative (iRIC) Software. Earth Surface Processes and Landforms, 45(1), 11-37, doi:10.1002/esp.4653, 2019.

Shimizu, Y., Osada, K., & Takanashi, T.: Numerical simulation of the driftwoods behavior by using a DEM-FLOW coupling model. Annual Journal of Hydraulic Engineering, JSCE, vol. 50, 787-792, 2006, (In Japanese).

https://doi.org/10.5194/esurf-2022-52
Preprint. Discussion started: 20 September 2022

Steeb, N., Rickenmann, D., Badoux, A., Rickli, C., & Waldner, P.: Large wood recruitment processes and transported volumes in Swiss mountain streams during the extreme flood of August 2005. Geomorphology, 279, 112-127, doi: 10.1016/j.geomorph.2016.10.011, 2017.

Swanson, F. J., Gregory, S. V., Iroumé, A., Ruiz-Villanueva, V., & Wohl, E.: Reflections on the history of research on large wood in rivers. Earth Surface Processes and Landforms, 46(1), 55-66, doi: 10.1002/esp.4814, 2021.

The River Sabo Technical Review Committee for the restoration on the Chikugo river right bank basin, Report on the Akatani river basin disaster, pp.67, 2018.

Yabe, T., Aoki, T., Sakaguchi, G., Wang, P. Y., & Ishikawa, T.: The compact CIP (Cubic-Interpolated Pseudo-particle) method as a general hyperbolic solver. Computers & Fluids, 19(3-4), 421-431, 1991.

Yamazaki, Y., & Egashira, S.: Run out processes of sediment and woody debris resulting from landslides and debris flow. Association of Environmental and Engineering Geologists; special publication 28, doi:10.25676/11124/173184, 2019.

https://doi.org/10.5194/esurf-2022-52
Preprint. Discussion started: 20 September 2022

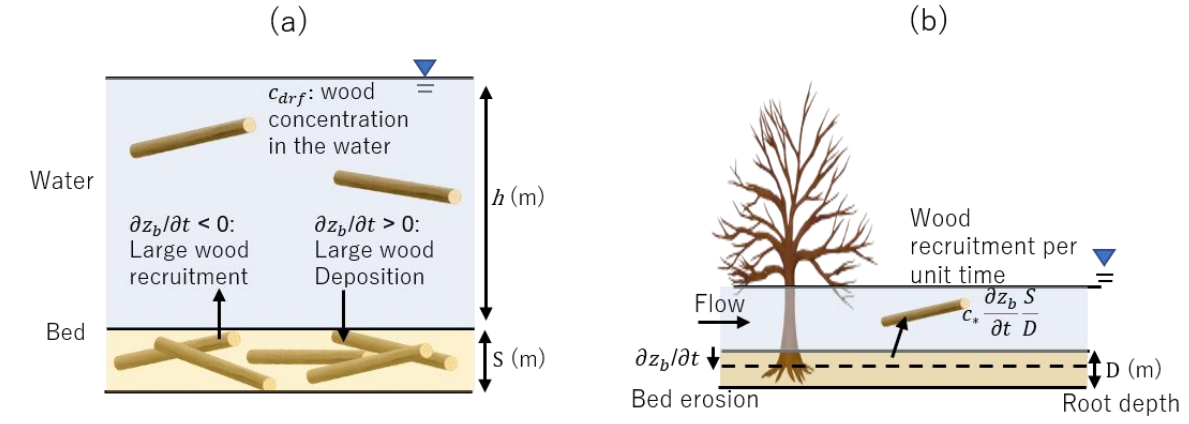

Figure 1: Concept of large wood recruitment and deposition (a), and the relation between bed erosion, rood depth and large wood recruitment (b).

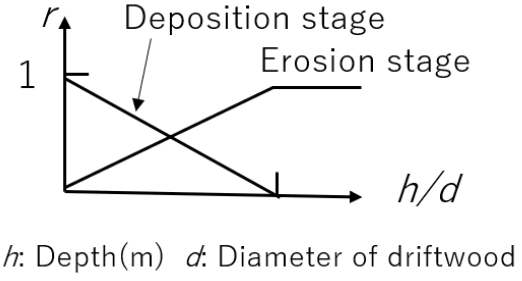

Figure 2: Specification of the functional form of $r(t, x, y)$

https://doi.org/10.5194/esurf-2022-52
Preprint. Discussion started: 20 September 2022

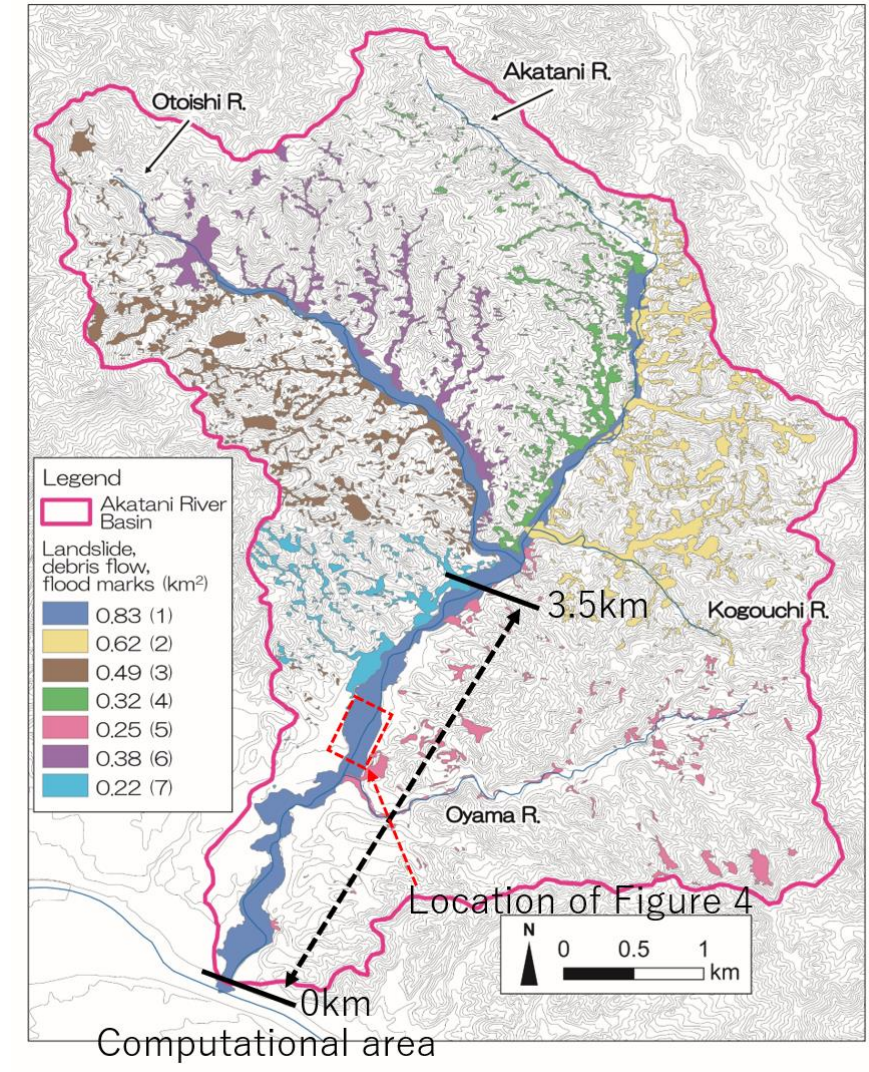

Figure 3: The Akatani River basin with debris flows and flood marks identified from aerial photos (Nagumo et al., 2019 was modified by the authors). The background image is provided by the Geographical Information Authority of Japan. The debris flows and flood marks are color-coded to identify the tendency of sediment supply: (1) is along the channels, (2) is the left bank side of the Akatani river basin, (3) is the right bank side of the Otoishi river basin, (4) is the right bank side of the Akatani river basin, (5) is the Oyama river basin, (6) is the left bank side of the Otoishi river basin, and (7) is the right bank side of the Akatani river basin.

https://doi.org/10.5194/esurf-2022-52
Preprint. Discussion started: 20 September 2022

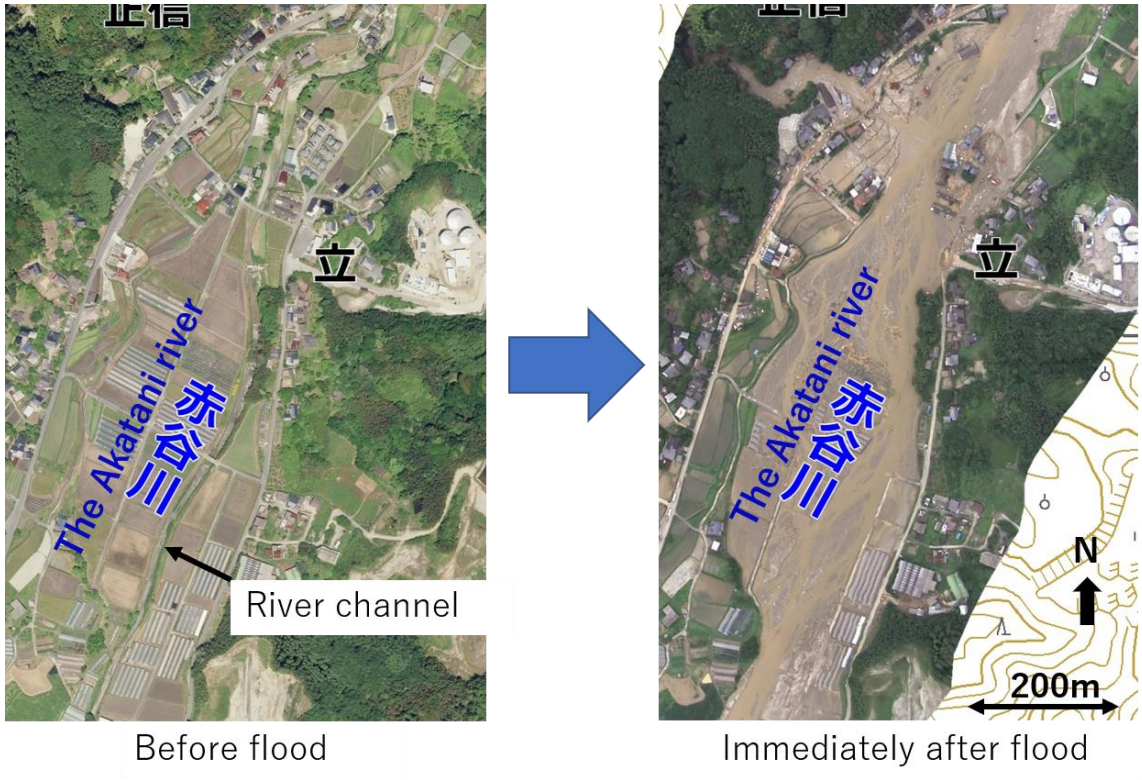

Figure 4: Aerial photos of the Akatani River before (left) and after (right) the flood event in July 2017. The background image provided by the Geographical Information Authority of Japan.

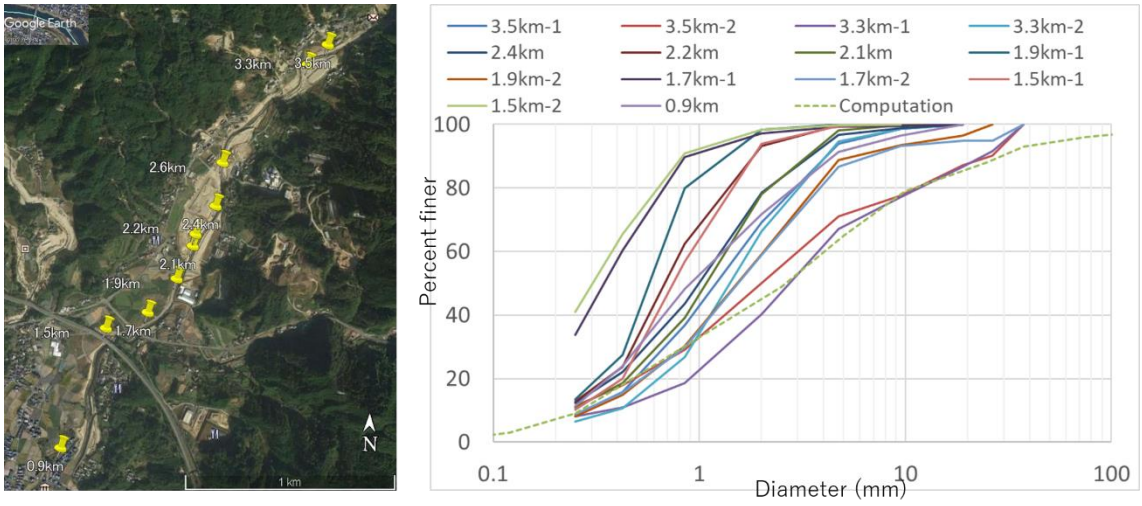

375 **Figure 5: Sediment sampling sites (left photo) and the sediment size distribution observed immediately after the flood event (right figure). The dotted line is employed as the initial condition in the computation. The background image was taken from © Google Maps.**

https://doi.org/10.5194/esurf-2022-52
Preprint. Discussion started: 20 September 2022

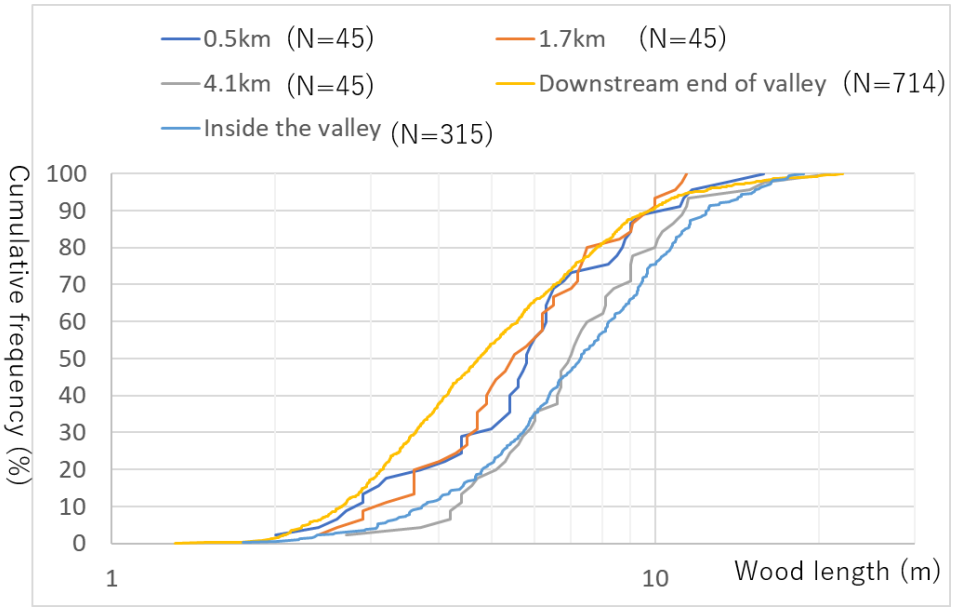

Figure 6: Distribution of wood length identified from aerial photos taken just after the event.

380

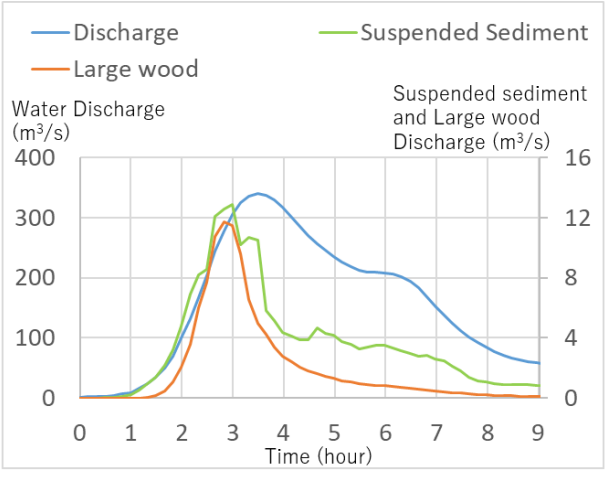

Figure 7: Computed results, i.e., upstream boundary conditions for 2-D computation, for flood water, suspended sediment, and large wood discharge at the 3.5 km point.

https://doi.org/10.5194/esurf-2022-52
Preprint. Discussion started: 20 September 2022

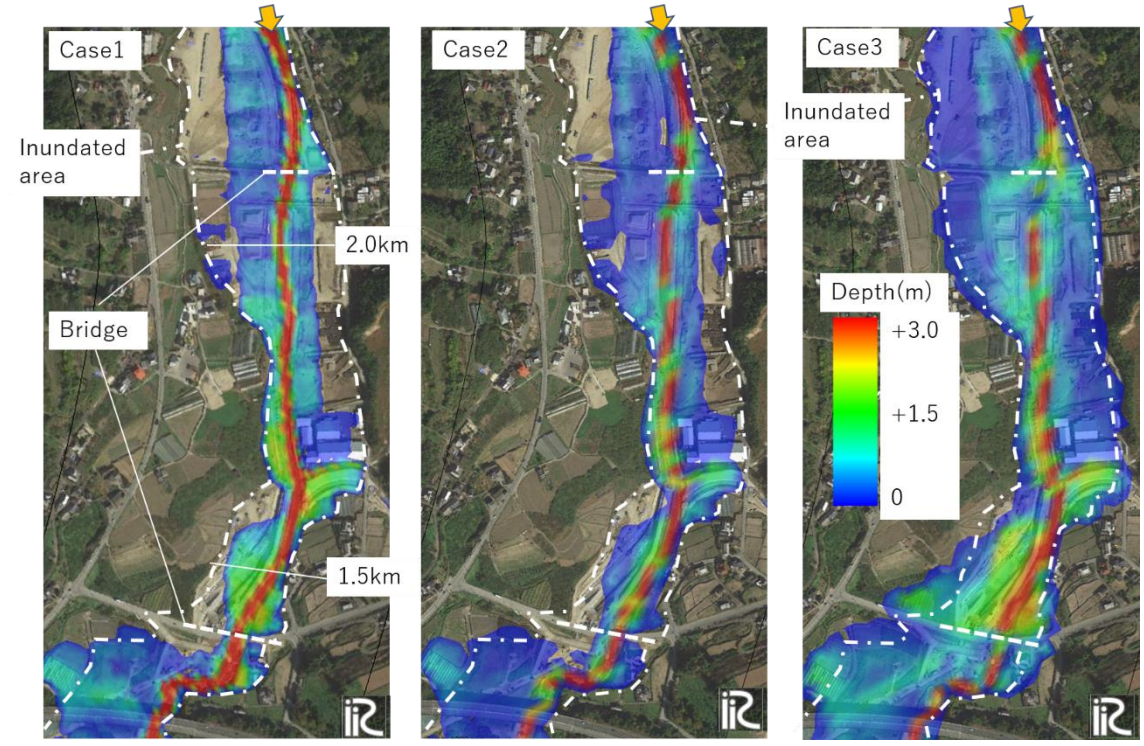

Figure 8: Comparison of water depth at peak discharge between Case 1 (left) , Case 2 (middle), and Case 3 (right). The white dotted line indicates the inundated area as deciphered from aerial photo. The background image was taken from © Google Maps.

https://doi.org/10.5194/esurf-2022-52
Preprint. Discussion started: 20 September 2022

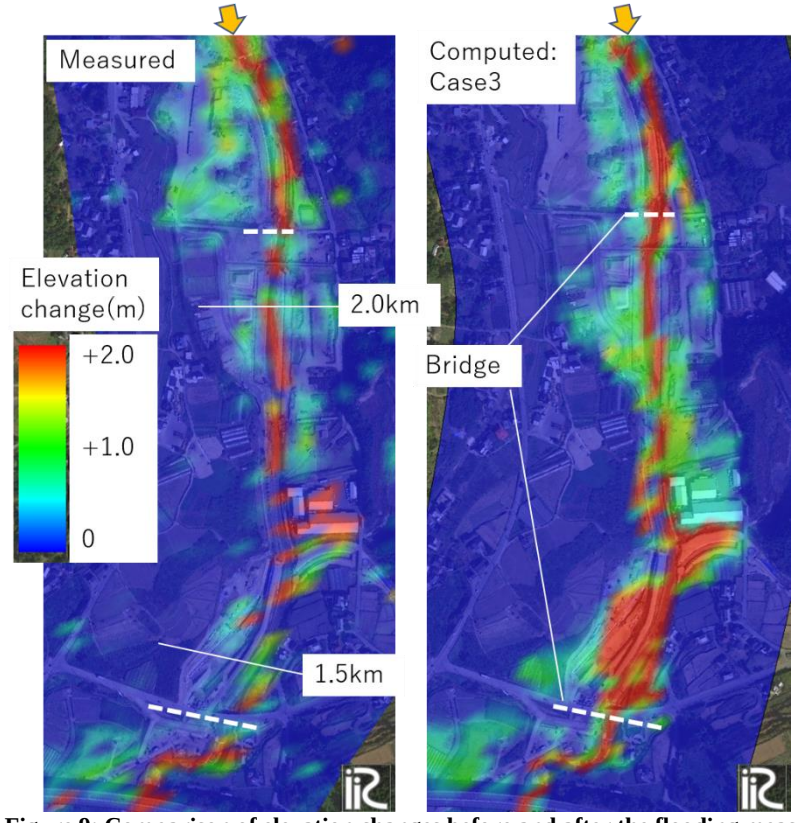

Figure 9: Comparison of elevation changes before and after the flooding measured by aerial laser survey (left) and elevation change at the end of Case 3 calculation (right). The background image was taken from © Google Maps.

https://doi.org/10.5194/esurf-2022-52
Preprint. Discussion started: 20 September 2022

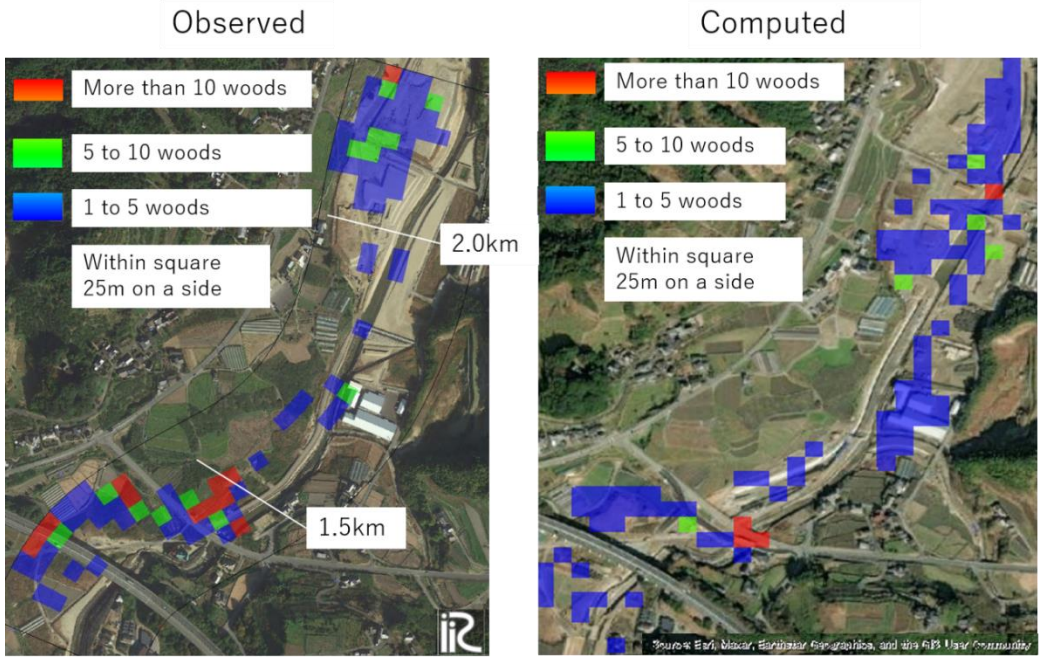

Figure 10: Comparison of the large wood deposition between the observed from the aerial photos (left) and computed results (right). The computed results are converted to the number of pieces of large wood by assuming that the diameter and length of a piece of wood are 20 cm and 7 m, respectively. The background image was taken from © Google Maps.

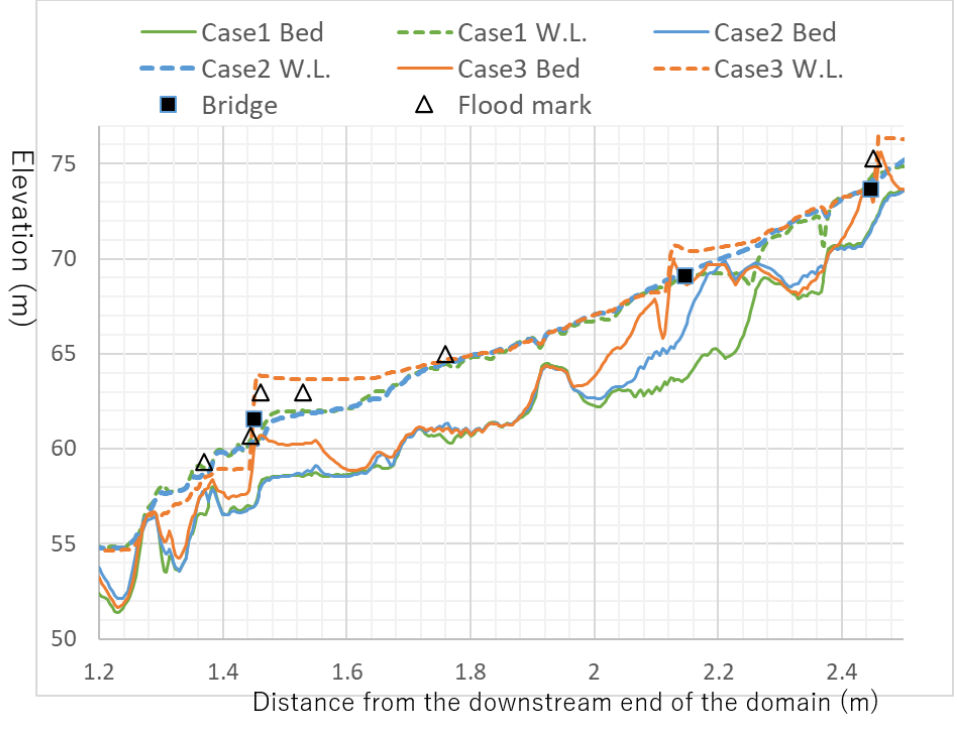

https://doi.org/10.5194/esurf-2022-52
Preprint. Discussion started: 20 September 2022

Earth Surface Dynamics Discussions
Open Access
EGU

Figure 11: Comparison of the results of each case with the water level mark and river bed elevation in the longitudinal direction of the river channel during peak flow. Bridge location ■ shows the elevation of the bridge height.

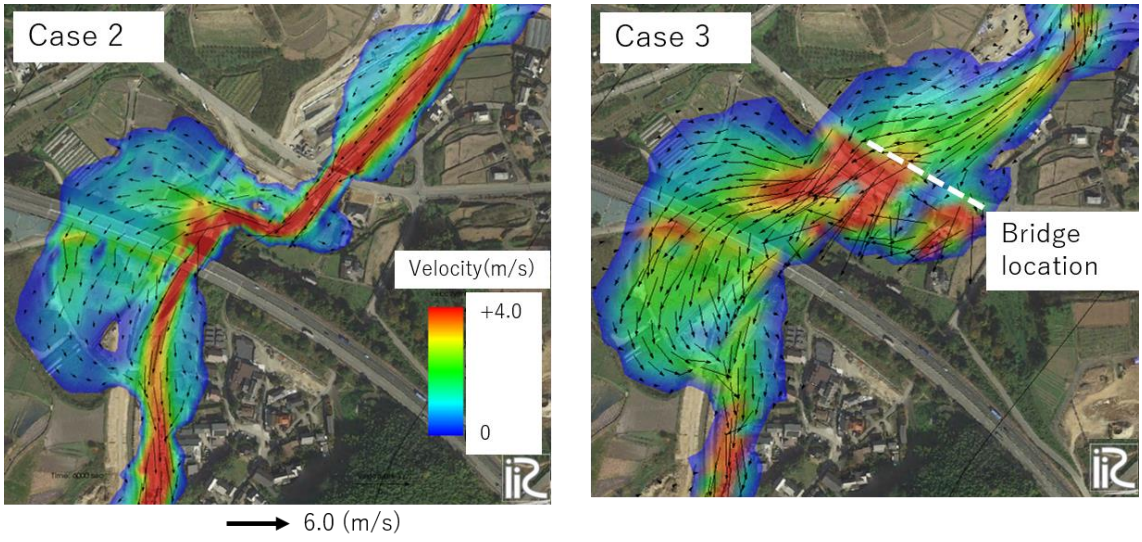

395 **Figure 12: Difference in flow pattern between Case 2 (left) and Case 3 (right) around the bridge at peak discharge. The background image was taken from © Google Maps.**

Table 1. Parameters employed for the rainfall-runoff and landslide computations.

Item	Value
Mesh size (m)	10×10
Soil depth (m)	1.0
Saturated hydraulic conductivity (cm/s)	0.5
Equivalent roughness coefficient	0.4
Soil porosity: λ	0.475
Internal friction angle (degrees)	35
Cohesion (kN/m^2)	12.5
Soil density (kg/m^3)	2650
Water density (kg/m^3)	1000

Table 2. Calculation conditions for the 2-D flood flow with sediment and large wood

Case 1	Flow only
Case 2	Flow with sediment, without large wood
Case 3	Flow with sediment and large wood